Hindawi Publishing Corporation
Physics Research International
Volume 2012, Article ID 836430, 11 pages
doi:10.1155/2012/836430

Review Article

Optical Second Harmonic Generation in Semiconductor Nanostructures

Tatiana V. Murzina,[1] Anton I. Maydykovskiy,[1] Alexander V. Gavrilenko,[2] and Vladimir I. Gavrilenko[2]

[1] *Faculty of Physics, Moscow State University, Moscow 119991, Russia*
[2] *Center for Materials Research, Norfolk State University, Norfolk, VA 23504, USA*

Correspondence should be addressed to Vladimir I. Gavrilenko, vgavrilenko@nsu.edu

Received 20 January 2012; Accepted 16 March 2012

Academic Editor: Goro Mizutani

Copyright © 2012 Tatiana V. Murzina et al. This is an open access article distributed under the Creative Commons Attribution License, which permits unrestricted use, distribution, and reproduction in any medium, provided the original work is properly cited.

Optical second harmonic generation (SHG) studies of semiconductor nanostructures are reviewed. The second-order response data both predicted and observed on pure and oxidised silicon surfaces, planar $Si(001)/SiO_2$ heterostructures, and the results related to the direct-current-and strain-induced effects in SHG from the silicon surfaces as well are discussed. Remarkable progress in understanding the unique capabilities of nonlinear optical second harmonic generation spectroscopy as an advanced tool for nanostructures diagnostics is demonstrated.

1. Introduction

In recent decades, optical techniques have been extensively used to study the size dependence of linear-, second-, and third-order optical nonlinearities of nanocrystals in relationship to the quantum confinement [1–4]. A remarkable progress has been achieved in studies of the effects of surfaces and interfaces in semiconductor nanostructures, nanowires, and nanoparticles (see [5] and references therein).

If a high-intensity beam of light strikes a specimen, the latter will respond in a nonlinear manner and higher optical harmonics will be generated in addition to the linear optical response. The strongest measurable nonlinear optical response is the second harmonic generation (SHG). The generated higher harmonics are functions of the specimen atomic structure. Most materials possess odd-order nonlinear optical susceptibility components; however, the even-order nonlinear susceptibility terms exist only in the systems having noncentrosymmetric atomic geometry [6–8]. Consequently, if the initial inversion symmetry of a reflecting system (like, e.g., bulk Si, Ge, C crystals, and/or centrosymmetric molecules, ideally shaped nanoparticles,) is for some reason broken, for example, due to crystal truncation, defects, external fields, and so forth, it results in even-order harmonics generation. Note that in central symmetric systems the SHG-active (and other even-order harmonics) areas are restricted by the symmetry reduction regions. In noncentral symmetric systems the symmetry reduced results in an appearance of initially forbidden optical susceptibility tensor components that can be experimentally detected. This extremely high sensitivity of the even-order nonlinear optical response (such as SHG) to the local symmetry makes it a very efficient tool for probing atomic and molecular processes on surfaces and interfaces. In nanostructures where the contribution of the surface-related effects to the total optical response is increasingly important with the size reduction, the unique symmetry sensitivity allows developing an efficient SHG-based nonlinear optical diagnostics probe, as demonstrated in this paper.

The development of the laser provided intense source of monochromatic and coherent light that stimulated extensive research and applications in the field of nonlinear optics [9]. Nonlinear optical microscopy has been used to study inorganic, organic, and biological materials [10] for decades. The advantages of the nonlinear microscopes include improved spatial and temporal resolution without the use of pinholes or slits for spatial filtering. In particular, for the applications in biology and medicine it has been demonstrated that

multiphoton excitation microscopy has the capacity to image deeper within highly scattering tissues such as *in vivo* human skin [10].

In this work we summarize some recent experimental and theoretical works on the SHG mostly related to the silicon nanostructures. The work is organized as follows. Section 2 describes the theoretical description of nonlinear optical response. Section 3 describes recent experimental studies of direct-current-(DC-) and strain-induced effects in SHG from crystalline silicon surface. Section 4 presents the experimental and theoretical results related to semiconductor superlattices.

2. Optical Response

Following the description of the electromagnetic (EM) field in materials, within its penetration depth beneath the surface, the incident light field at the frequency $\omega(E(\omega))$ induces different order optical susceptibilities $\chi^{(n)}$ [5, 11]. The linear polarization is given by [3].

$$P_i(\omega) = \chi_{ij}^{(1)} E_j(\omega). \tag{1}$$

The second-order polarization is given by [3]

$$\begin{aligned} P_i(2\omega) = {} & \chi_{ijk}^{(2)D} E_j(\omega) E_k(\omega) \\ & + \chi_{ijkl}^{(3)Q} E_j(\omega) \nabla_k E_l(\omega) \\ & + \chi_{ijkl}^{(3)\mathrm{EFISH}} E_j(\omega) E_k(\omega) E_l^{\mathrm{DC}}(0). \end{aligned} \tag{2}$$

Equation (1) represents linear optics. Nonlinear optical response, originating from anharmonic bond polarizabilities, governs Second Harmonic Generation and is determined through several contributions given by (2) [12], all of them being caused by noncentrosymmetric distortion of crystalline lattice. The first term in (2) describes the second-order optical excitation process and vanishes in centrosymmetric systems (like bulk Si) in the electric dipole approximation. The second term, which is proportional to the field gradient (∇E), is the electric quadrupole component (in magnetic materials it contains also a magnetic dipole component). External electric field (if present), E^{DC}, breaks the central symmetry thus inducing the SHG and higher even-order nonlinear response. For example, in bulk Si (and other cubic solids having inversion symmetry) only the two last terms in (2) contribute to the SHG resulting in a very weak signal [3].

The nonlocal (local-field effects) and many body (exciton) contributions can cause substantial corrections to the SHG spectra [11]. Moreover, it has been demonstrated theoretically that additional subjections like direct current (DC) or mechanical strain can further decrease the symmetry of silicon thus giving rise to additional, current-induced, and strain-induced components of nonlinear polarization, that is discussed in Section 3.

3. Direct-Current- and Strain-Induced Second Harmonic Generation in Silicon

This section is focused on an SHG generation in centrosymmetric systems as the result of the symmetry reduction due to the external electrical and mechanical fields.

3.1. Direct-Current-Induced SHG in Si(001). The effect of field-induced nonlinearity in centrosymmetric medium like silicon has been studied both experimentally and theoretically. Electric- and magnetic-field-induced effects in SHG are being extensively explored for the diagnostics of surfaces, interfaces, and nanostructures [13, 14]. Less studied was a phenomenon of the inversion symmetry break as the result of an external electrical direct current (DC). This effect can play an important role in SHG from the silicon surface. In this case, the current-induced distortion of the electron equilibrium distribution function in a quasi-pulse domain causes the dipole-like second-order nonlinearity that exists in the region affected by the DC.

The first theoretical description of the current-induced SHG (CSHG) was presented in [15], where the CSHG contribution to the nonlinear polarization for a direct band semiconductor was discussed. The CSHG contribution to $\vec{P}_{2\omega}$ can be introduced in a similar manner to the electric field induced SHG and given by

$$P_i^{\mathrm{DC}}(2\omega) = \chi_{ijkl}^{(3)\mathrm{DC}} E_j(\omega) E_k(\omega) j_l(0), \tag{3}$$

where j is the current density and $\hat{\chi}^{(3)\mathrm{DC}}$ is the dipole current-induced optical susceptibility. In case of direct semiconductors an asymmetry of the electron quasi-pulse distribution leads to the appearance of a current-induced term in second-order susceptibility with a sharp resonance in the vicinity of the local Fermi level, E_F, for majority carriers in the conduction band. It follows from symmetry considerations that $\hat{\chi}^{(3)\mathrm{DC}}(j)$ is an *odd* function of current density, $\hat{\chi}^{(3)\mathrm{DC}}(j) = -\hat{\chi}^{(3)\mathrm{DC}}(-j)$. This shows a possibility for an experimental observation of DC-induced effects in SHG, which was first studied in [16].

Figure 1(a) shows a schematic view of the structure used for CSHG studies. Nickel electrodes were thermally evaporated on top of p-Si(001) ($\rho \sim 10^{-3}\,\Omega$cm) that was used as a substrate. The $200 \pm 20\,\mu$m wide gap between Ni electrodes was oriented along y crystallographic axis as it is shown in the figure; ohmic resistance of Ni/Si contact was $\approx 0.02\,\Omega$. It has been proved that the temperature of the sample during the CSHG measurements was less than 40°C.

CSHG experiments were carried out using the output of a tunable Ti: sapphire laser (wavelength range $710 \div 850$ nm, pulse duration of 80 fs, average power of 130 mW, repetition rate of 86 MHz) as the fundamental radiation. The laser beam was focused onto the Si(001) surface between the Ni-electrodes with a spot size of $40\,\mu$m in diameter. SHG radiation was filtered out by appropriate set of filters and detected by a PMT and gated electronics.

Special care has been taken to avoid the influence of the DC-induced heating and strain-induced effects on the CSHG measurements. To that end, only the s-polarization of both

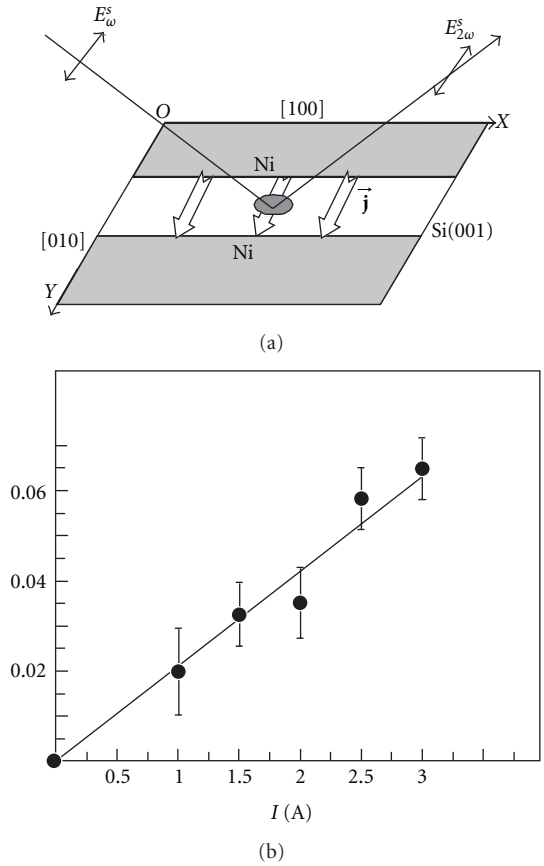

Figure 1: (a) Schematic view of the experimental scheme for current-induced *s*-in, *s*-out SHG. (b) Dependence of the CSHG contrast on the DC value for the fundamental wavelength of 780 nm (adapted from [16]).

the pump and the SHG beams was used, because it is well known that only bulk quadrupole susceptibility contributes to the second harmonic signal in that case [18]. Eightfold symmetric anisotropic SHG dependence was observed for this polarization-related geometry configuration. The azimuthal Si(001) orientation resulted in zero SHG intensity that was chosen as a reference for the measurements, because all the SHG contributions from Si vanish for the symmetry reasons, except those caused by the CSHG [16].

In order to reveal the CSHG effect, an external SHG homodyne source (30 nm thick ITO film) was used and the *odd* character of the dependence $\hat{\chi}^{(3)\mathrm{DC}}$ on (j) was exploited. It is important to note that, under the chosen experimental geometry only transversal DC, where $j \| (OY)$, gives rise to a nonzero SHG signal while it vanishes for the longitudinal geometry, where $j \| (OX)$. Thus the total detected SHG intensity from the sample and the reference depends on the current density and direction and can be described by the expression [16]

$$I_{2\omega} \propto \left| \mathbf{E}^{\mathrm{ref}}_{2\omega} + \mathbf{E}^{\mathrm{sample}}_{2\omega}(j) \right|^2, \tag{4}$$

where $\mathbf{E}^{\mathrm{samp}}_{2\omega}(j) = E^{\mathrm{samp}}_{2\omega}(j)\exp(i\phi^{\mathrm{samp}})$ and $\mathbf{E}^{\mathrm{ref}}(2\omega) = E^{\mathrm{ref}}_{2\omega}\exp(i\phi^{\mathrm{ref}})$ are complex amplitudes of the current-induced

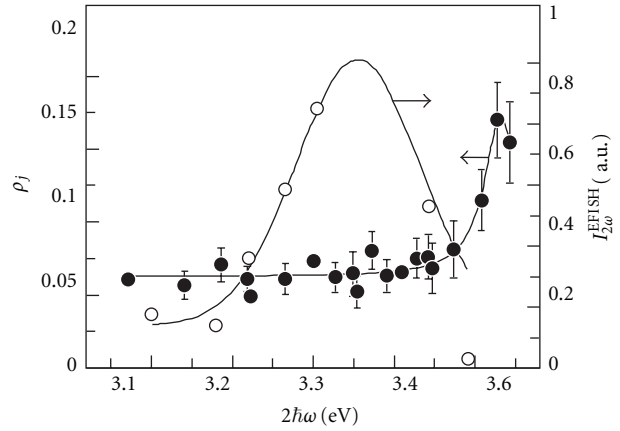

Figure 2: Spectroscopy of the CSHG contrast measured for $I = 4\,A$ (filled circles) and of EFISH intensity (open circles) (adapted from [17]).

and current-independent SH fields from the sample and the reference, respectively; $E^{\mathrm{samp}}_{2\omega}(j)$, $E^{\mathrm{ref}}_{2\omega}$, ϕ^{samp}, and ϕ^{ref} are real amplitudes and phases of SH fields, respectively. Interference of the two components of the SH field in (4) results in the appearance of a homodyne cross-term in the SHG intensity that changes its sign under current reversal and leads to *odd* in j changes in the SHG intensity.

The DC-induced SHG can be characterized by the CSHG contrast according to [16]

$$\rho_{2\omega}(j) = \frac{I^{+}_{2\omega}(j,r) - I^{-}_{2\omega}(j,r)}{I^{\mathrm{ref}}_{2\omega}} \propto 4E^{\mathrm{ref}}_{2\omega}E^{\mathrm{samp}}_{2\omega}(j)\cos[\Delta\phi], \tag{5}$$

where $\Delta\phi$ is determined by the dispersion of air at ω and 2ω, the distance between the sample and the reference and the phases ϕ^{ref} and ϕ^{samp}.

Figure 1(b) shows the CSHG contrast dependence on j measured for a fixed position of the reference SHG sample. The measured linear character of $\rho_{2\omega}(j)$ dependence is in agreement with (5) and proves that the *odd* DC-induced SHG is observed. Moreover, the obtained results also prove that the heating has a negligible effect, as otherwise it should bring the even in j contribution to the SHG.

The only SHG source which can disguise the CSHG effect under the chosen experimental conditions was the electric-field-induced SHG (EFISH). It cannot be avoided by a certain choice of the experimental geometry because the symmetries of CSHG and EFISH are the same. Nevertheless there are at least two pieces of evidence that prove that $\rho_{2\omega}(j)$ dependence reflected the DC influence on nonlinear-optical signal from Si [16].

First, the CSHG intensity spectrum was compared with the EFISH that was measured on p-Si(001) [17] (Figure 2). One can see that EFISH spectrum shows a maximum at $2\hbar\omega \approx 3.34$ eV that is close to the E_1 resonance in silicon. At the same time, the CSHG contrast does not have resonant features in this spectral region that proves that observed CSHG effect was neither induced by the quadrupole nonlinearity nor by EFISH. In contrast, the increase

of the CSHG data at $2\hbar\omega \approx 3.5\,\text{eV}$ is in a qualitative agreement with the theoretical predictions [15].

Theoretical study of the EFISH DC-induced effect in SHG from Si(001) under external electric fields gave a value of the CSHG contrast at least two orders of magnitude lower than observed experimentally. The comparison of the CSHG intensity to that measured in Si(001) and to the SHG intensity observed in crystalline quartz with well-known values of the second-order susceptibility allowed the estimation of the maximum value of DC-induced susceptibility in silicon to be $\hat{\chi}^{(2)\text{DC}}(j_{\max}) \approx 3 \cdot 10^{-15}\text{m/V}$.

3.2. Strain-Induced SHG in Si(001). Recently the strain-induced SHG in silicon surface has been observed by several groups [19–22]. The physical mechanism of strain-induced nonlinearity is determined by the breaking of the intrinsic inversion symmetry of Si under mechanical deformation and consequently by a modification of the electronic spectrum.

Most of the efforts were concentrated on the studies of internal strain that may exist at Si/SiO_2 interfaces; however the modification of the SHG intensity as a function of the external biaxial strain was reported in [22]. The measurements were performed using the experimental laser setup described in the previous section. As a target, the n-doped (4.5 Ωcm) 0.5 mm thick Si(100) plate was used. The strain was applied by pressing the back side of the Si plate by a metallic sphere fixed at the end of a micrometric stage while a movable base supplies the formation of strain in the Si wafer as is shown; in Figure 3(a). The optically probed depth of Si subsurface layer was about 30 to 50 nm and the deformation was considered to be uniform. This means that the crystalline symmetry of Si(001) can be considered to be undistorted; therefore the strain-induced SHG modification caused by the symmetry changes can be neglected.

The biaxial strain of the subsurface layer corresponds to the spherical deformation geometry as shown in Figure 3(b) [22]. Figure 3(c) shows modification of SHG spectrum from silicon under biaxial strain observed at the conditions close to the mechanical break threshold (open circles) compared to the free plate SH spectrum (solid circles) [22]. The deformation of the Si wafer was about 100 μm that corresponded to the mechanical stress of 350 MPa. P-polarizations of the fundamental and SHG waves were chosen in such a way that this combination of polarizations corresponded to the maximal strain-induced effect in SHG. It can be seen that both spectra have maxima with the energy locations corresponding to the SHG photon energy of $2\hbar\omega \approx 3.3\,\text{eV}$ that is close to the energy of the direct electron transitions near E_1 and E_0' critical points of the Si band structure. Slight variations of the SHG line shape as well as of the SHG intensity were also observed [22].

To characterise qualitatively the strain-induced modulation of the SHG intensity the strain-induced SHG (SSHG) contrast can be described as

$$\rho_{2\omega}(\sigma) = \frac{I_{2\omega}(0) - I_{2\omega}(\sigma)}{I_{2\omega}(\sigma)}, \tag{6}$$

where $I_{2\omega}(0)$ and $I_{2\omega}(\sigma)$ are the SHG intensities measured for zero and nonzero value of the strain, σ. Figure 4 shows

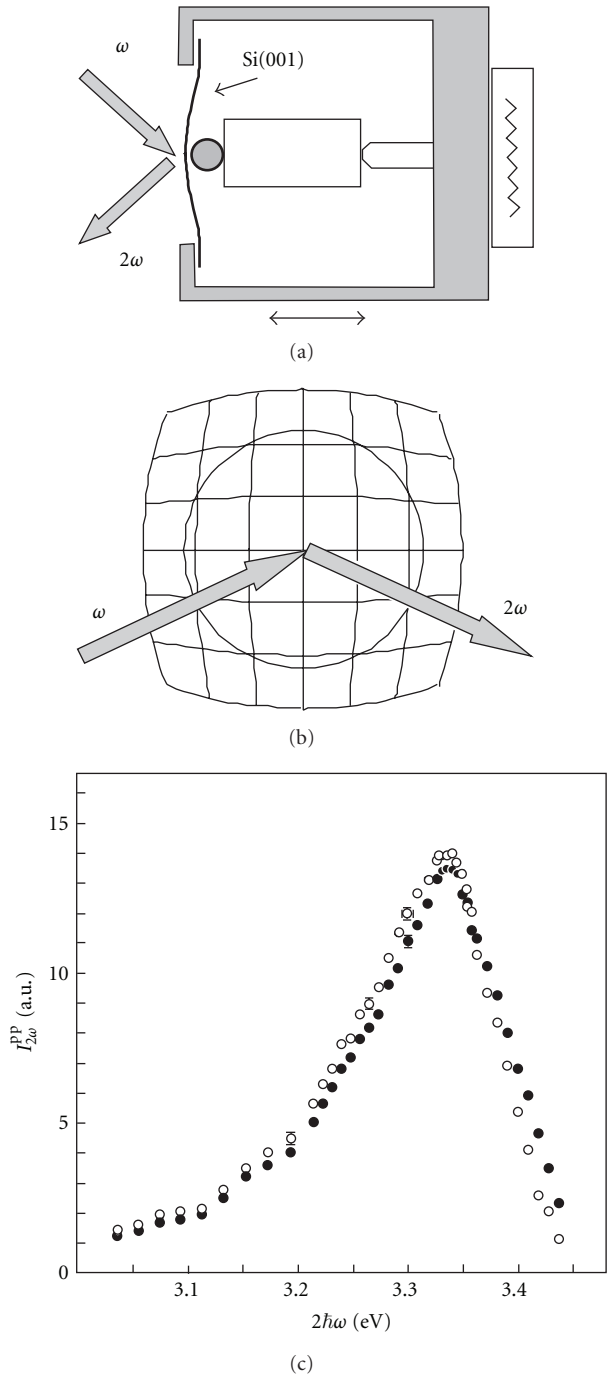

Figure 3: (a) Setup of the strain-induced SHG experiments; (b) schematic view of the biaxial strain of Si(001) surface; (c) SHG spectrum of the zero strain (filled circles) and under the biaxial deformation (open circles) n-doped (4.5 Ωcm) 0.5 mm thick Si(100) plate (adapted from [22]).

the dependencies of the SSHG contrast on σ measured for different fundamental wavelengths. It can be seen that up to the Si (001) deformation value of $1.6 \cdot 10^{-3}$ the SSHG contrast corresponds to the second-order polynomial dependence in

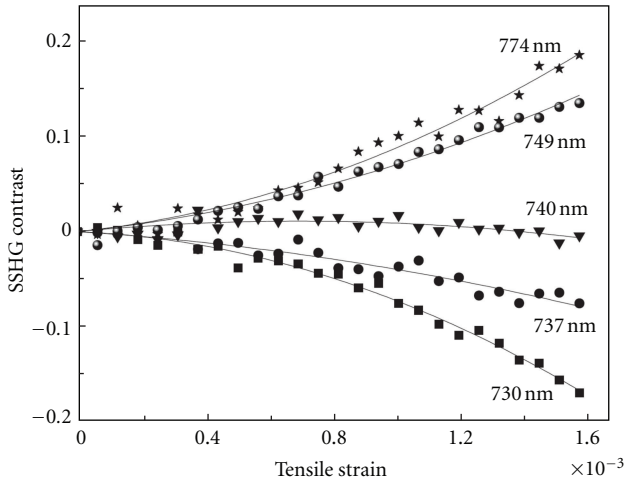

FIGURE 4: SSHG contrast measured for different wavelengths as a function of the biaxial deformation (adapted from [22]).

agreement with the possible theoretical description of strain-induced SHG [22]:

$$I_{2\omega} \propto \left|\mathbf{E}^0_{2\omega} + \mathbf{E}_{2\omega}(\sigma)\right|^2 \approx \left(E^0_{2\omega}\right)^2 + 2E^0_{2\omega}E_{2\omega}(\sigma), \quad (7)$$

where $E_{2\omega}(\sigma) \propto p_{ijklm}\sigma_{lm}$, p_{ijklm} is the piezo-optical tensor. It can be seen that SSHG curves change their slope sign as the fundamental wavelength is tuned through the E_1/E_0' Si critical point of combined density of states at 3.33 eV. The results demonstrate a strong strain-induced effect in SHG from the silicon surface.

The possible mechanisms of the observed effects can be the strain-induced shifts of the conduction and valence bands, similarly to the linear case [24], or by modification of the charge distribution in the crystal and in dioxide charge traps. The latter mechanism corresponds to the EFISH at the Si/SiO_2 interface; the corresponding static electric field is perpendicular to the silicon surface that can produce an isotropic SHG. At the same time it was proved that the application of a uniaxial strain along the orthogonal in-plane direction *OX* and *OY* resulted in different modifications of the reflected SHG. This supports the conclusion of the possibility to detect the strain-induced nonlinearities induced by mechanical distortions of the silicon structure that really was observed experimentally [22].

4. Second Harmonic Generation from Semiconductor Surfaces and Nanostructures

Increasing amount of high-quality research on nonlinear optical properties of nanocrystals within the past decade is caused by extensive developments of nanotechnology, nanophotonics, and nanoelectronics [5] presenting with unique possibilities for SHG optical metrology and analysis of the nanocrystals. Numerous results obtained within past decades clearly demonstrate how important are the contributions of surface optical excitations to the overall nonlinear

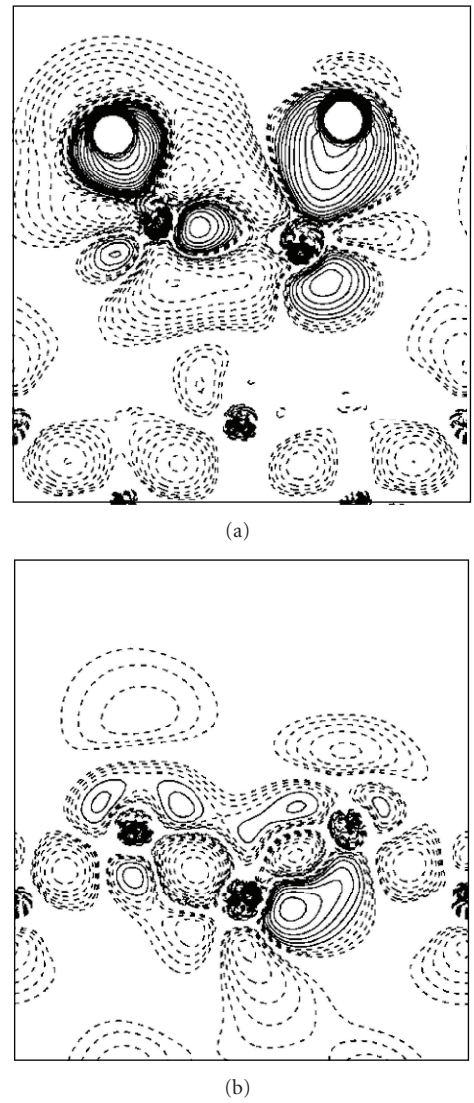

FIGURE 5: Calculated valence charge-density differences between bare and unrelaxed monohydride Si(001)(2 × 1) surface: $\rho_{\text{bare}} - \rho_{\text{mono}}$. The charge maps are cut through two vertical $[1\bar{1}0]$ planes located at $Y = 0$ (a) and $Y = a_y$ (b) in the unit cell. Contours start from $\pm 1 \times 10^{-3}$ e/a.u.^{3} and increase successively by a factor of $\sqrt{2}$. Dashed (solid) lines indicate charge accumulation (depletion) in the electron density (adapted from [23]).

response of nanostructures. This section is focused on the SHG from surfaces and interfaces in nanostructures.

As stated before SHG is extremely sensitive to the surfaces in cubic materials [25–27]. One of the reasons for that is the evidence that in centrosymmetric crystals the SHG response is forbidden by symmetry in bulk but allowed on the surface where the local symmetry is lower [25].

One can clearly see in Figure 5 that plotted charge redistribution causing induced bond asymmetries (thus allowing SHG by reduction of inversion symmetry) involves only few atomic monolayers near the surface. This demonstrates extreme locality of the SHG response that makes it very promising for the diagnostics of nanostructures.

Demonstrated strong localization of nonlinear optical response is very important in view of the progress in the developments of the nanoparticles combined from crystalline materials (core) and organic molecules. Several studies of such systems indicated dominant contributions of optical excitations in the interfaces regions [5].

A recent surge in the number of Si-SiO_2 system studies within the past few years has been caused by extensive developments of nanostructured electronics which requires a fundamental understanding of the processes at the atomic monolayer scale. Understanding of the oxygen-related processes on Si-SiO_2 interface is very important for both fundamental and applied physics as well as for the high-tech electronics.

For contactless optical characterization of the interface at nanometer scale the nontraditional methods of optical spectroscopy are used: linear optical reflectance differential spectroscopy (RDS), see [28–31] and references therein, and/or nonlinear optical spectroscopy of second harmonic generation. Development of the next generation of optical metrology will require the detailed interpretation of optical spectra based on microscopic modelling and simulations. The first principle calculations of SHG [3, 32] of silicon-based interfaces allowed substantial progress in our understanding of the physics and chemistry of the systems. However such works are still rare (in particular those related to the SHG) because they normally require extensive large scale computations [3, 32].

Atomic structure of the intermediate Si and SiO_2 layer is extensively debating in the literature [33, 34]. Monte Carlo simulations [33] and first principle modelling based on density functional theory (DFT) and total energy minimization method [34] confirmed ordered Si-O-Si bridge structure as a basic unit of the intermediate SiO_2 layer. On the other hand the Rutherford ion scattering data measured on the Si-SiO_2 interface and interpreted using the *ab initio* DFT study with modified interatomic potential [35] suggested substantial contribution of disordered interface structure. It should be noted that optical spectra are very sensitive to the structural disorder, which smears out well-pronounced atomic order-related features. The SHG spectra measured on the systems containing single [36] or multiple Si(001)-SiO_2 interfaces (multiple Si-SiO_2 quantum wells, [37]) showed appearance of new SHG feature in the spectral region near 2.7 eV [37] and 3.8 eV [36, 37] that could not be interpreted in terms of the perturbations of the Si bulk-like direct electron gaps.

Realistic modelling of optical functions of solid surfaces and interfaces still remains challenging for the first principle theories [3, 30, 31]. Description of excited states which could be in good agreement with experiment normally requires inclusion of local field, many-body (excitonic) effects, and probably other nonlocal contributions (in particular for SHG) [38, 39]. This makes theory much more complicated than frequently used independent particles approach (or Random Phase Approximation, RPA). The nonlinear SHG response from the surfaces and interfaces is more challenging for the *ab initio* theory even within the RPA method because of the more complicated unit cell. Consequently first principles studies of the SHG from solid surfaces are still rare (see [3, 32, 39] and references therein).

In [26] the first principle computational analysis of nonlinear SHG optical spectra of Si-SiO_2 interface has been performed. Results of the work demonstrated the possibility of unambiguously identifying well-pronounced spectral features in SHG optical spectra of the Si-SiO_2 interface with local atomic oxygen-related configurations. Equilibrium atomic structures of Si(001)-SiO_2 interface are obtained from the total energy minimization method within DFT using *ab initio* norm-conserving [40, 41] and ultrasoft (VASP, [42]) pseudopotentials (PPs).

Calculated self-consistent eigenenergies and eigenfunctions are used as inputs for optical calculations. Within its penetration depth beneath the surface, the incident light field at frequency $\omega(E(\omega))$ induces different order optical susceptibilities $\chi^{(n)}$ that determine linear- (1) and second-order (2) polarization.

The (2×2) unit cell has been used to model the clean Si(001) surface. It has been demonstrated before that this model realistically reproduces most significant features of electronic structure and RDS spectra of bare Si(001) surface [3, 31, 44]. Initial oxidation stage of the Si(001) is characterized mainly by two local atomic configurations including oxygen atom: oxygen dimer bridge and oxidized backbonds configurations (see Figure 6 [28–31, 44, 45] and references therein). Fully relaxed atomic structure of hydrogenated Si(001)(2×2) surface with one local oxygen dimer bridge configuration per cell is shown in Figure 7(a).

Calculated value of the dimer length of 3.13 Å on hydrogenated surface is slightly bigger then the value of 3.06 Å obtained by [31] on Si(001)(2×2) surface without hydrogen. Equilibrium geometry of bridge oxygen located in a broken backbond of monohydride Si(001) surface is shown in Figure 7(b).

The length of the oxidized backbond on hydrogenated surface, 2.93 Å, is higher than the value of 2.61 Å obtained on a bare surface. The last data agree well with those reported earlier in the literature: 2.53 Å [31], 2.60 Å [45].

The calculated tridymite atomic configuration of SiO_2 is used as a basic structural model for initial oxide layer in Si(001) surface. The fully relaxed atomic geometry of the Si(001)-SiO_2 interface is shown in Figure 8. Atomic structure presented in Figure 8 corresponds to the reported earlier atomic configuration for the tridymite [34, 46].

It has been demonstrated [30, 43, 47–49] that SHG is a unique method to study centrosymmetric solid surfaces: the SHG response is forbidden in bulk, and the SHG signal is generated within only a few surface monolayers. Because of that one can expect stronger contribution of oxygen-related process in Si(001)-SiO_2 interface to the SHG spectra than in linear optics.

The calculated SHG efficiency spectra are now compared with available experimental data. The SHG spectra measured on Si(001) surface with native oxide [48] and on Si(001)-SiO_2 with potassium- and NaCl-covered oxides (in order to study electric field effect in the space charge region) [34] indicate strong dependence of the signal on the surface electric field and appearance of a new optical structure in

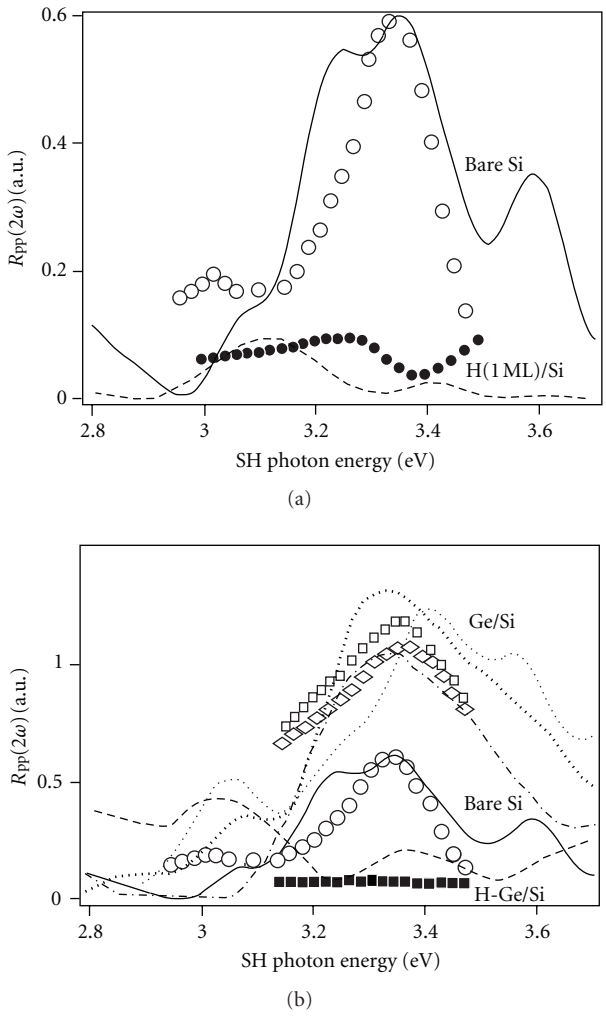

FIGURE 6: Comparison of calculated and measured SHG spectra for P-in/P-out configuration. (a) Clean Si(001) (2×1), theory (solid curve) and experiment(open circles); Si(001) (2×1): H monohydride, theory (dashed curve) and experiment (filled circles). Note strong quenching, red-shifting, and line shape distortion of 3.35 eV (E_1) peak in both theory and experiment, (b) Clean Si(001) (2×1), theory (solid curve) and experiment (open circles) as in (a), Si(001) : Ge(1 ML), theory (dot-dashed curve) and experiment (diamonds); Si(001) : Ge(2 ML), theory (heavy dotted curve: fully relaxed structure; light dotted curve: reduced buckling structure) and experiment (open squares); Si(001) : Ge(2 ML) with saturation H-coverage, theory (dashed curve) and experiment (filled squares) (adapted from [43]).

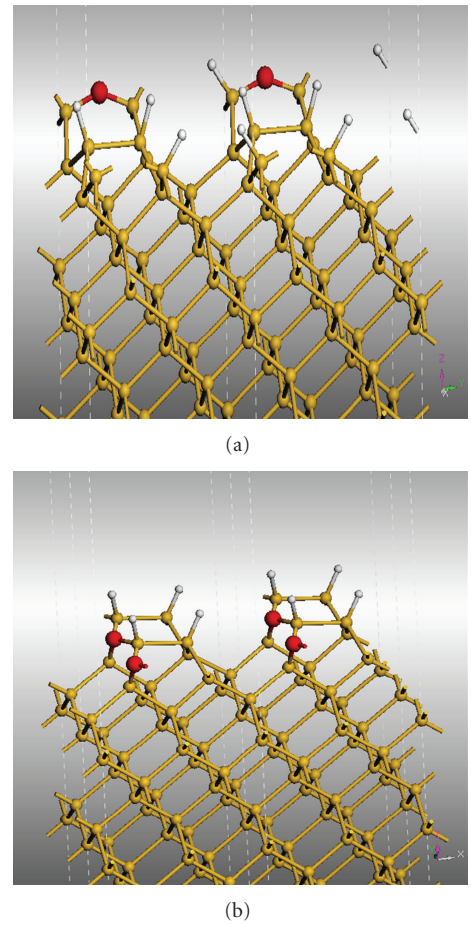

FIGURE 7: Atomic structure of Si(001)(2×2) surface with one local dimer oxygen configuration per unit cell (a) and atomic structure of Si(001)(2×1) surface with an oxygen atom located on a broken back bond. (b) Red and white colored balls correspond to oxygen and hydrogen atoms, respectively (adapted from [26]).

the region 3.6 to 3.8 eV. Electric-field-induced SHG (EFISH) offers incredible possibilities for new generation of optical metrology of the interfaces because of the high sensitivity of the SHG signal to the surface electric field [35, 46]. From a theoretical prospective, however, the microscopic theory of EFISH is nonlocal, and it is still challenging to model for the first principle theory [30, 44]. EFISH was beyond the scope of the study by [26].

Here we are focused on the effect of the chemical nature of electronic bond contributions on Si(001)-SiO_2 interface to the SHG. Figure 9 presents the calculated SHG spectra of Si(001)-SiO_2 interface shown in Figure 8.

As expected the nonzero SHG response is predicted only in the spectral region corresponding to optical two-photon excitations of the near-surface located disturbed Si electron orbitals. Due to the high value of Si–O bond energy corresponding contributions are located in far ultraviolet region. The SHG response from the Si–SiO_2 interface located mostly in visible and near-UV regions is attributed to the distorted host atomic bonds [25, 30, 43]. From the data presented in Figure 9 one can immediately extract features related to the oxygen. Removal of the bridge oxygen results in dramatic reductions of the SHG features near 2.7, 3.3, 3.8 to 4.0, and 5.1 eV. Comparison between relaxed and unrelaxed structure calculations of the SHG efficiency (upper and lower panel in Figure 9, resp.) shows a more pronounced effect of mechanical stress in SHG than in RDS spectra (see Figure 9). The SHG features near 3.3 and 5.1 eV are close to the bulk electron transitions E_1 and E_1'.

Note that the theory with the QP correction predicted critical point energies in Si slab at $E_1 = 3.4$ eV, $E_2 = 4.15$ eV,

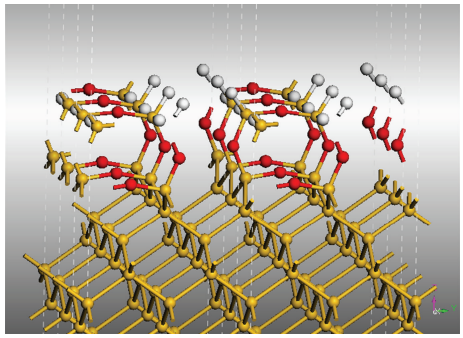

Figure 8: Fully relaxed atomic configuration of Si(001)-SiO_2 interface. Dashed lines indicate unit cells. Red and white coloured balls correspond to oxygen and hydrogen atoms, respectively (adapted from [26]).

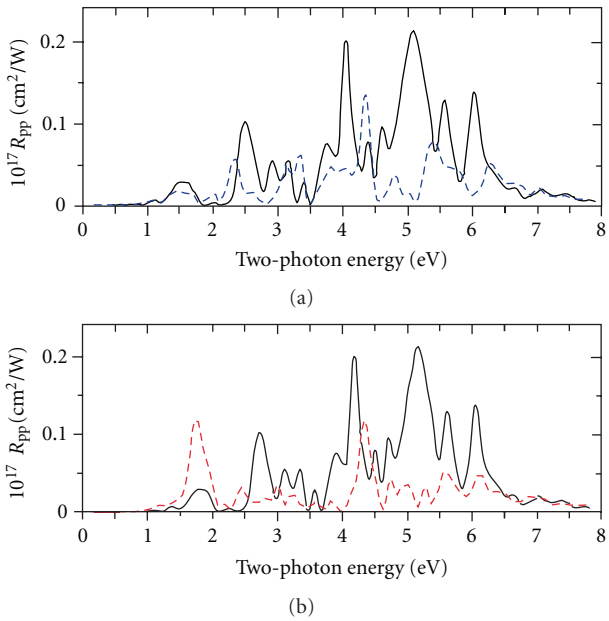

Figure 9: Calculated Second Harmonic Generation efficiency spectra of the Si(001)-SiO_2 interface corresponding to the geometry given in Figure 8 (solid line) are shown in comparison to the SHG spectra calculated after removal of the bridge oxygen (dashed line). Fully relaxed (a) (unrelaxed (b)) atomic structure of the Si(001)-SiO_2 interface is used for optical calculations (adapted from [26]).

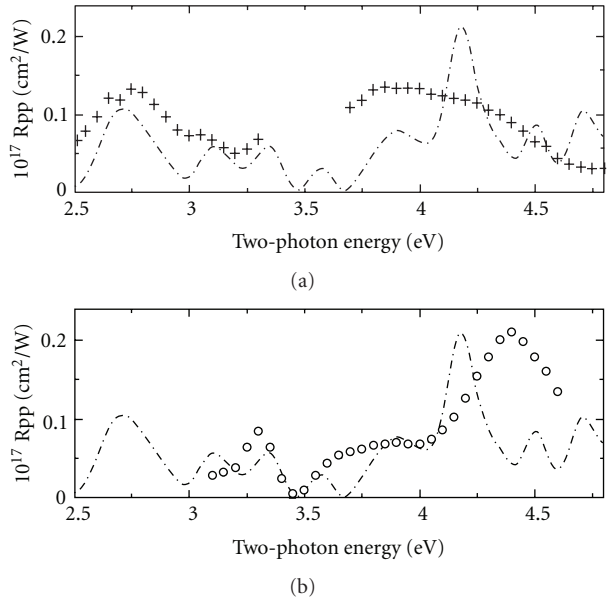

Figure 10: The calculated second harmonic generation efficiency spectra of the relaxed Si(001)-SiO_2 geometry given in Figure 8 are shown in comparison to experimental data. In (a) the calcualted spectrum (dashed) is compared to data (symbols) measured by Avramenko et al. in [37]. (b) compares the theoretical spectrum (dashed) to experimental data (symbols) measured by Rumpel et al. in [36] (adapted from [26]).

and $E_1' = 5.0$ eV. The peaks near 3.3 and 5.1 eV apparently relate to the bulk-like electron excitations. According to [26] the SHG response near 5.1 eV exhibits strongest sensitivity to oxygen. This spectral region however is still unavailable for experimental study.

The SHG peak near 1.8 eV is of the surface nature related to the Si dimer bond. This peak is strongly affected by oxygen and local stress (see Figure 9). One can expect that it will also be sensitive to the size of nanoparticles since the smaller the particle, the higher the curvature of the interface and the more stress that is introduced at the Si/SiO_2 interface [50, 51]. Contribution of oxygen in this region is clearly shown in RDS spectra in this spectral region however effect of the stress relaxation is much less important in RDS than in SHG. The SHG peaks located near 2.7 eV and 3.8 eV are new and they are not predicted on the Si surfaces without oxygen. According to the analysis of PDOS spectra these peaks are directly related to the Si backbonds of the dimer atoms hybridized to the bridge oxygen $2p$-electrons. Peak near 4.0 eV is close to the E_2 transition and it is strongly affected by the new feature near 3.8 eV. Comparison between SHG efficiency predicted for relaxed and unrelaxed tridymite structure after removal of bridge oxygen (upper and lower panels in Figure 8, resp.) demonstrates that effects of local stresses and bond rehybridization are equally important in SHG which is in contrast to the linear optical RDS response [28].

The predicted SHG efficiency spectrum of oxidized Si(001) surface is compared next with available experimental data [35, 36, 48].

In Figure 10 a comparative analysis of the SHG spectra measured on two different systems is presented: the Si(001) surface oxidized [36] or with natural oxide [49] and Si-SiO_2 multiple quantum well structure [37]. In order to compare the shape of the predicted and measured SHG spectra the amplitudes of experimental data were scaled to meet the theoretical values at 4.2 eV (lower panel) and at 2.7 eV (upper panel).

The experimental SHG spectrum shown in the upper panel in Figure 9 was measured by [36] on Si(001) sample with 10 nm oxide layer grown by thermal oxidation at 1000°C. The dominant SHG peak at 4.3 eV was attributed to the E_2 bulk transitions [36]. Note that the theoretical bulk

value of $E_2 = 4.15$ eV underestimates experimental one by about 0.1 eV. The results shown in Figure 10 indicate the appearance of a new SHG response in the region of 3.6 to 4.0 eV and a strong enhancement of the E_2 peak. Comparison with the SHG data presented in Figure 9 indicates that this is caused by the combined effect of the oxygen-related rehybridization of Si backbonds and structural reconfiguration. The strong enhancement of both measured and predicted SHG efficiencies caused by boron doping of the Si(001) surface (which was obtained on the relaxed system) was reported earlier [46]. In both cases by neglect of the electric field effect, the physical nature of the predicted strong enhancement of the SHG efficiency is impurity related to the rehybridization and structural reconfiguration of the Si backbonds.

New predicted SHG response near 3.6 to 4.0 eV is also accompanied by dramatic increase of the calculated SHG efficiency at 2.7 eV due to the dimer bridge oxygen (see Figures 9 and 10). This part of the predicted SHG spectra agrees well with another type of experimental results by [37] where a strong SHG signal in the region near 2.7 eV on Si(001)-SiO_2 multiple quantum wells (MQWs) was measured. The four MQW systems studied by [37] were fabricated from Si-layers of the thicknesses equal to 1.0, 0.75, 0.5, and 0.25 nm separated by SiO_2 films of fixed 1.1 nm thicknesses. The number of Si-SiO_2 MQW bilayers varied from 30 to 70 in order to provide nearly the same thickness of the whole film stuck [37].

In MQW system the quantum size effect is an additional factor affecting the SHG. However in the presence of multiple Si(001)-SiO_2 boundaries the effect of the interface oxygen should be substantially enhanced. In the absence of microscopic theory the 2.7 eV SHG signal measured in Si(001)-SiO_2 MQW was interpreted by [37] as a result of electron transitions from the bound quantum electron states in QW. In addition to the quantum size effect, the chemical nature of the last SHG feature was also suggested by [37] as an alternative interpretation of their data. The results of the present work suggest that the origin of the feature measured by [37] and the predicted SHG responses near 2.7 eV is a dominant contribution of the rehybridized and reconstructed Si backbonds due to creation of the dimer bridge oxygen structure on Si(001)-SiO_2 interface. Additional argument towards the current interpretation of the 2.7 eV signal is that this response should be accompanied by the SHG features near 3.8 eV as discussed above (see Figure 9). Experimental data of [37] confirm this rule: in addition to the 2.7 eV SHG peak, the authors reported strong SHG response around 3.8 to 4.0 eV which is discussed above.

Analysis of the atom- and orbital-resolved projected electron density of states (PDOSs) calculated in [26] clearly indicate a strong effect of the bridge oxygen which results in additional contribution (hybridization) of oxygen p-orbitals and silicon backbond orbitals. The $2p$-orbitals of bridge oxygen contribute to the top of the valence band. Modifications of the c-band are less pronounced. The rehybridization of the host valence electron orbitals caused by both $2p$-orbitals of oxygen and by structural distortions seems to be responsible for the measured and predicted optical anisotropy of this system. The dominating effect in optical anisotropy of Si(001) due to the distorted backbonds and additional hybridization to oxygen has been shown by [30].

5. Conclusions

This paper reviews a progress in understanding the second harmonic generation spectroscopy for diagnostics of semiconductor surfaces and nanostructures. The unique capabilities of the SHG metrology is caused by its extreme sensitivity to the symmetry of the optically excited systems. Another property of the SHG is related to the substantial contributions of the nonlocal processes caused by electric, mechanical and magnetic fields.

It should be noted that effects of external fields (like electric field, direct current induced SHG, Electric-Field-Induced SHG) and eventually many-body (excitonic) and local field effects [5, 11] should be incorporated by interpretation of the SHG in order to achieve more detailed quantitative description of the signal shape which should be considered as a future activity road map in the field. For future experimental and theoretical studies it is important to explore the unique sensitivity of SHG to symmetry and external fields that should make the SHG metrology an advanced diagnostics tool for nanostructures.

Acknowledgments

T. V. Murzina and A. I. Maydykovskiy gratefully acknowledge O. A. Aktsipetrov, A.A. Nikulin, O. V. Bessonov, A. A. Fedyanin, and T. V. Dolgova for the long-term collaboration in the reviewed area; financial support from RFBR (Grant 10-02-01136). A. V. Gavrilenko and V. I. Gavrilenko acknowledge support of NSF PREM DRM-0611430, NSF NCN EEC-0228390, AFOSR FA9550-09-1-0456, and NSF CREST-1036494.

References

[1] R. A. Ganeev, M. Baba, M. Morita et al., "Nonlinear optical properties of CdS and ZnS nanoparticles doped into zirconium oxide films," *Journal of Optics A*, vol. 6, no. 4, pp. 447–453, 2004.

[2] M. Jacobsohn and U. Banin, "Size dependence of second harmonic generation in CdSe nanocrystal quantum dots," *Journal of Physical Chemistry B*, vol. 104, no. 1, pp. 4–5, 2000.

[3] M. C. Downer, B. S. Mendoza, and V. I. Gavrilenko, "Optical second harmonic spectroscopy of semiconductor surfaces: advances in microscopic understanding," *Surface and Interface Analysis*, vol. 31, no. 10, pp. 966–986, 2001.

[4] J. E. Sipe and R. W. Boyd, "Nanocomposite materials for nonlinear optics based on local field effect," in *Optical Properties of Nanostructured Random Media*, V. M. Shalaev, Ed., p. 1, Springer, Berlin, Germany, 2002.

[5] V. I. Gavrilenko, *Optics of Nanomaterials*, Pan Stanford, Singapore, 2011.

[6] N. Bloembergen, *Nonlinear Optics*, Benjamin, New York, NY, USA, 1965.

[7] R. W. Boyd, *Nonlinear Optics*, Academic Press, 1992.

[8] Y. R. Shen, *The Principles of Nonlinear Optics*, Wiley, 2nd edition, 2003.

[9] N. Bloembergen, "Nonlinear optics and spectroscopy," *Reviews of Modern Physics*, vol. 54, no. 3, pp. 685–695, 1982.

[10] B. R. Masters and P. T. C. So, "The genesis of nonlinear microscopies and their impact on modern development," in *Handbook of Biomedical Nonlinear Optical Microscopy*, B. R. Masters and P. T. C. So, Eds., p. 5, Oxford University, Oxford, UK, 2008.

[11] E. Luppi, H. Hübener, and V. Veniard, "Ab initio second-order nonlinear optics in solids: second-harmonic generation spectroscopy from time-dependent density-functional theory," *Physical Review B*, vol. 82, no. 23, Article ID 235201, 15 pages, 2010.

[12] J. E. Sipe and E. Ghahramani, "Nonlinear optical response of semiconductors in the independent-particle approximation," *Physical Review B*, vol. 48, no. 16, pp. 11705–11722, 1993.

[13] Y. R. Shen, "Surface properties probed by second-harmonic and sum-frequency generation," *Nature*, vol. 337, no. 6207, pp. 519–525, 1989.

[14] R. P. Pan, H. D. Wei, and Y. R. Shen, "Optical second-harmonic generation from magnetized surfaces," *Physical Review B*, vol. 39, no. 2, pp. 1229–1234, 1989.

[15] J. Khurgin, "Current induced second harmonic generation in semiconductors," *Applied Physics Letters*, vol. 67, no. 8, Article ID 1113, 3 pages, 1995.

[16] O. Aktsipetrov, V. Bessonov, A. Fedyanin, and V. Valdner, "DC-induced generation of the reflected second harmonic in silicon," *JETP Letters*, vol. 89, no. 2, pp. 58–62, 2009.

[17] O. Aktsipetrov, A. Fedyanin, A. Melnikov et al., "Dc-electric-field-induced and low-frequency electromodulation second-harmonic generation spectroscopy of Si(001)-SiO_2 interfaces," *Physical Review B*, vol. 60, no. 12, pp. 8924–8938, 1999.

[18] H. W. K. Tom, T. F. Heinz, and Y. R. Shen, "Second-harmonic reflection from silicon surfaces and its relation to structural symmetry," *Physical Review Letters*, vol. 51, pp. 1983–1986, 1983.

[19] S. Govorkov, V. Emel'yanov, N. Koroteev, G. Petrov, I. Shumay, and V. Yakovlev, "Inhomogeneous deformation of silicon surface layers probed by second-harmonic generation in reflection," *Journal of the Optical Society of America B*, vol. 6, no. 6, pp. 1117–1124, 1989.

[20] J. Huang, "Probing inhomogeneous lattice deformation at interface of Si(111)/SiO_2 by optical second-harmonic reflection and Raman spectroscopy," *Japanese Journal of Applied Physics A*, vol. 33, no. 7, pp. 3878–3886, 1994.

[21] S. Govorkov, N. Koroteev, G. Petrov, I. Shumay, and V. Yakovlev, "Laser nonlinear-optical probing of silicon/SiO_2 interfaces: surface stress formation and relaxation," *Applied Physics A*, vol. 50, no. 4, pp. 439–443, 1990.

[22] O. Aktsipetrov, V. O. Bessonov, T. Dolgova, and A. Maidykovskii, "Second harmonic generation induced by mechanical stresses in silicon," *JETP Letters*, vol. 90, no. 11, pp. 718–722, 2009.

[23] V. I. Gavrilenko, R. Q. Wu, M. C. Downer, J. G. Ekerdt, D. Lim, and P. Parkinson, "Optical second-harmonic spectra of Si(001) with H and Ge adatoms: first-principles theory and experiment," *Physical Review B*, vol. 63, no. 16, Article ID 165325, 8 pages, 2001.

[24] P. Etchegoin, J. Kircher, and M. Cardona, "Elasto-optical constants of Si," *Physical Review B*, vol. 47, no. 16, pp. 10292–10303, 1993.

[25] V. I. Gavrilenko, "Ab initio theory of second harmonic generation from semiconductor surfaces and interfaces," *Physica Status Solidi A*, vol. 188, no. 4, pp. 1267–1280, 2001.

[26] V. I. Gavrilenko, "Differential Reflectance and Second Harmonic Generation from Si-SiO_2 Interface from First Principles," *Physical Review B*, vol. 77, Article ID 155311, 2008.

[27] V. I. Gavrilenko, "Optics of Nanostructured Materials from First Principle Theories," in *Tutorials in Complex Photonic Media*, M. A. Noginov, G. Dewar, M. W. McCall, and N. I. Zheludev, Eds., chapter 15, pp. 479–524, SPIE Press, Bellingham, WA, USA, 2009.

[28] Y. Borensztein, O. Pluchery, and N. Witkowski, "Probing the Si-Si dimer breaking of Si(100)2×1 surfaces upon molecule adsorption by optical spectroscopy," *Physical Review Letters*, vol. 95, no. 11, Article ID 117402, 4 pages, 2005.

[29] T. Yashuda, S. Yamasaki, M. Nishizawa et al., "Optical anisotropy of oxidized Si(001) surfaces and its oscillation in the layer-by-layer oxidation process," *Physical Review Letters*, vol. 87, no. 3, Article ID 037403, 4 pages, 2001.

[30] F. Fuchs, W. G. Schmidt, and F. Bechstedt, "Understanding the optical anisotropy of oxidized Si(001) surfaces," *Physical Review B*, vol. 72, no. 7, Article ID 075353, 2005.

[31] A. Incze, R. Del Sole, and G. Onida, "Ab initio study of reflectance anisotropy spectra of a submonolayer oxidized Si(100) surface," *Physical Review B*, vol. 71, no. 3, Article ID 35350, 7 pages, 2005.

[32] H. Sano and G. Muzitani, "Ab initio calculation of surface nonlinear optical response," *E-Journal of Surface Science and Nanotechnology*, vol. 1, pp. 57–66, 2003.

[33] Y. Tu and J. Tersoff, "Microscopic dynamics of silicon oxidation," *Physical Review Letters*, vol. 89, Article ID 086102, 4 pages, 2002.

[34] R. Buczko, S. J. Pennycook, and S. T. Pantelides, "Bonding arrangements at the Si-SiO_2 and SiC-SiO_2 interfaces and a possible origin of their contrasting properties," *Physical Review Letters*, vol. 84, no. 5, pp. 943–946, 2000.

[35] A. Bongiorno, A. Pasquarello, M. S. Hybertsen, and L. C. Feldman, "Transition structure at the Si(100)-SiO_2 interface," *Physical Review Letters*, vol. 90, no. 18, Article ID 186101, 4 pages, 2003.

[36] A. Rumpel, B. Manschwetus, G. Lilienkamp, H. Schmidt, and W. Daum, "Polarity of space charge fields in second-harmonic generation spectra of Si(100)/SiO_2 interfaces," *Physical Review B*, vol. 74, no. 8, Article ID 081303, 2006.

[37] V. G. Avramenko, T. V. Dolgova, A. A. Nikulin et al., "Subnanometer-scale size effects in electronic spectra of Si/SiO_2 multiple quantum wells: interferometric second-harmonic generation spectroscopy," *Physical Review B*, vol. 73, no. 15, Article ID 155321, 2006.

[38] V. I. Gavrilenko and F. Bechstedt, "Optical functions of semiconductors beyond density-functional theory and random-phase approximation," *Physical Review B*, vol. 55, no. 7, pp. 4343–4352, 1997.

[39] R. Leitsmann, W. G. Schmidt, P. H. Hahn, and F. Bechstedt, "Second-harmonic polarizability including electron-hole attraction from band-structure theory," *Physical Review B*, vol. 71, no. 19, Article ID 195209, 13 pages, 2005.

[40] M. Fuchs and M. Scheffer, "Ab initio pseudopotentials for electronic structure calculations of poly-atomic systems using density-functional theory," *Computer Physics Communications*, vol. 119, no. 1, pp. 67–98, 1999.

[41] N. Troullier and J. L. Martins, "Efficient pseudopotentials for plane-wave calculations," *Physical Review B*, vol. 43, no. 3, pp. 1993–2006, 1991.

[42] G. Kresse and J. Furthmüller, "Efficiency of ab-initio total energy calculations for metals and semiconductors using a plane-wave basis set," *Computational Materials Science*, vol. 6, no. 1, pp. 15–50, 1996.

[43] V. I. Gavrilenko, R. Q. Wu, M. C. Downer, J. G. Ekerdt, D. Lim, and P. Parkinson, "Optical second harmonic spectra of silicon-adatom surfaces: theory and experiment," *Thin Solid Films*, vol. 364, no. 1-2, pp. 1–5, 2000.

[44] W. G. Schmidt, F. Bechstedt, and J. Bernholc, "Terrace and step contributions to the optical anisotropy of Si(001) surfaces," *Physical Review B*, vol. 63, no. 4, Article ID 045322, pp. 1–7, 2001.

[45] T. Uchiyama and M. Tsukada, "Atomic and electronic structures of oxygen-adsorbed Si(001) surfaces," *Physical Review B*, vol. 53, no. 12, pp. 7917–7922, 1996.

[46] A. Pasquarello, M. S. Hybertsen, and R. Car, "Si 2*p* core-level shifts at the Si(001)-SiO_2 interface: a first-principles study," *Physical Review Letters*, vol. 74, no. 6, pp. 1024–1027, 1995.

[47] J. L. P. Hughes and J. E. Sipe, "Calculation of second-order optical response in semiconductors," *Physical Review B*, vol. 53, no. 16, pp. 10751–10763, 1996.

[48] D. Lim, M. C. Downer, J. G. Ekerdt et al., "Optical second harmonic spectroscopy of boron-reconstructed Si(001)," *Physical Review Letters*, vol. 84, no. 15, pp. 3406–3409, 2000.

[49] G. Erley and W. Daum, "Silicon interband transitions observed at Si(100)-SiO_2 interfaces," *Physical Review B*, vol. 58, no. 4, pp. R1734–R1737, 1998.

[50] F. Bechstedt, *Principles of Surface Physics*, Springer, Berlin, Germany, 2003.

[51] K. W. Kolasinski, *Surface Science: Foundation of Catalysis Nanoscience*, Wiley, New York, NY, USA, 2nd edition, 2008.

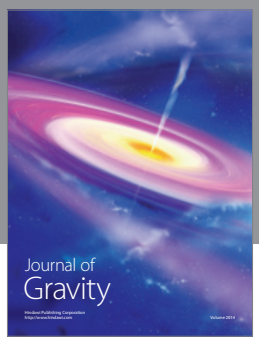

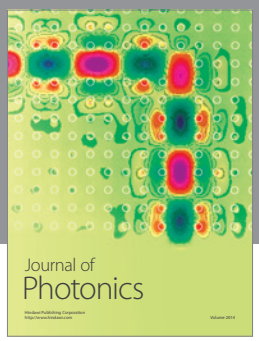

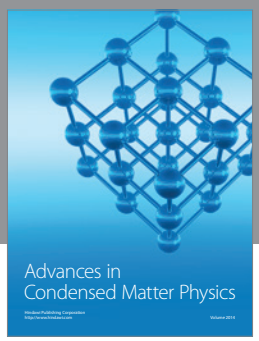

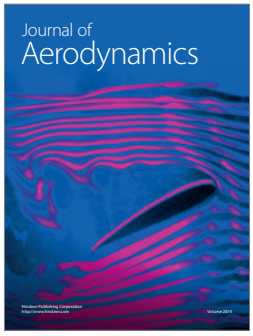

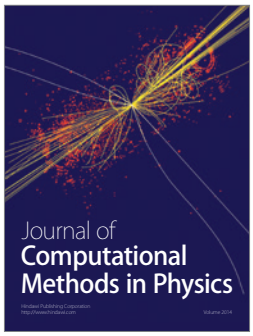

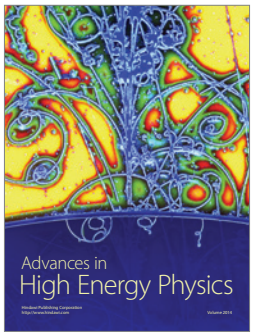

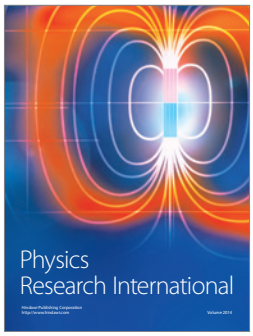

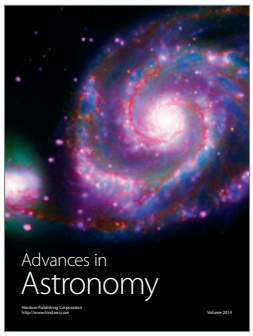

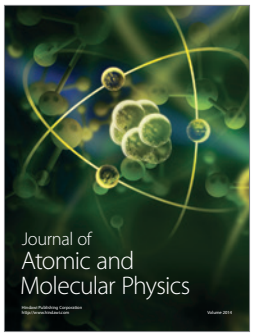

Hindawi

Submit your manuscripts at
http://www.hindawi.com